Th N104 04

Efficient 3D Frequency-domain Full-waveform Inversion of Ocean-bottom Cable Data - Application to Valhall in the Visco-ac

S. Operto* (GeoAzur), A. Miniussi (OCA), R. Brossier (University Joseph Fourier), L. Combe (Geoazur), N. Haller (BP), E. Kjos (BP), L. Métivier (LJK - ISTerre - CNRS), R. Milne (BP), A. Ribodetti (Geoazur - IRD), Z. Song (BP), J. Virieux (University Joseph Fourier) & Y. Zheng (BP)

SUMMARY

We present an application of 3D VTI visco-acoustic frequency-domain full waveform inversion (FWI) based on sparse direct solver on wide-azimuth OBC data from the Valhall oil field. Mono-parameter inversion for the vertical wavespeed is applied to the hydrophone component in the 3.5-10Hz passband. Compared to reflection traveltime tomography, we show the significant resolution improvement provided by FWI in the velocity reconstruction down to the base cretaceous reflector located below the reservoir level. This improvement was achieved although the presence of gas in the overburden. The FWI models are assessed by frequency-domain and time-domain modeling. We show an excellent match between recorded and modeled monochromatic gathers up to 10Hz. Time-domain modeling highlights the fit of the main diving and reflection arrivals interpreted in the data. We discuss the pros and cons of the frequency-domain formulation of FWI in terms of computational efficiency compared to time-domain FWI. In particular, we show the efficiency of the frequency-domain approach to process a large number of shots collected by fixed-spread acquisitions with a limited number of nodes of parallel computers. Perspectives are the use of block low-rank version of the direct solver to push inversion at higher frequencies and multi-parameter reconstruction including density, attenuation and epsilon.

Introduction

Full waveform inversion (FWI) has known a renew of interest in the oil industry since computational resources have become sufficient to perform 3D applications. However, the high computational demand still requires the designing of computationally efficient FWI algorithms. The most widespread implementation of 3D FWI is performed in the time domain (Tarantola, 1984), the main issue being to perform efficiently seismic modeling for thousands of sources. An obvious speedup strategy is to distribute the sources over the processors of parallel computers. Ideally, the source distribution requires at least as many processors as sources, and hence requires huge parallel computers. This source parallelism can be complemented by MPI subsurface domain decomposition or multithreading for loop parallelism. Reduction of data dimensionality have been proposed to mitigate this computational burden, either by random source encoding (Krebs et al., 2009) or subsampling (Warner et al., 2013).

Alternatively, full waveform modeling and inversion can be performed in the frequency domain (Pratt, 1999). The forward problem is a boundary value problem which requires the resolution of a large, sparse system of linear equations relating the seismic source to the monochromatic wavefield. This approach is worth of interest when wide-azimuth long-offset acquisitions allow performing FWI with a limited number of discrete frequencies. Among the possible approaches to solve the linear system, Gauss elimination methods based on sparse direct solver have the advantage of being efficient to process a large number of right-hand sides (i.e., sources). The efficiency of this approach has been extensively demonstrated with 2D case studies, while the memory demand of the LU decomposition of the system matrix has been considered for a long time as a major bottle neck.

The aim of this study is to question this last statement and to illustrate with a real data case study the efficiency of 3D frequency-domain FWI to process ocean bottom seismic data data in the visco-acoustic VTI approximation with limited computational resources.

Method: VTI visco-acoustic frequency-domain FWI

A conventional data-domain frequency-domain FWI is performed by iterative minimization of the least-squares misfit between the recorded and modeled pressure data. A multiscale FWI proceeds successively from low frequencies to the higher ones to mitigate the nonlinearity of the inversion. Monochromatic pressure wavefields are modeled in the visco-acoustic VTI approximation using a finite-difference frequency-domain method (Operto et al., 2014). The linear system resulting from the discretization of the time-harmonic wave equation is solved with the sparse direct solver MUMPS (MUMPS-team, 2011). The gradient of the misfit function with respect to the vertical wavespeed is computed with the adjoint-state method. A preconditioned steepest-descent method provides the descent direction at each iteration, while the amount of descent is estimated by a conventional line search. The preconditioning is built with the diagonal terms of the so-called pseudo Hessian. No regularization is used in this study. The source signature estimation is alternated with the subsurface update during each nonlinear FWI iteration.

Application to OBC data from Valhall

We apply the 3D frequency-domain FWI to the hydrophone component of a 4C OBC data set collected in the Valhall oil field. The Valhall field is a shallow-water giant field in the North Sea characterized by gas-charged sediments in the overburden, forming locally a gas cloud between 1km and 1.5km depth (Sirgue et al., 2010). The subsurface is also characterized by a significant anisotropy, which reaches a maximum value of 16%. The reservoir is located at 2.5km depth and shows evidence of compaction under production. We used the same dataset as that processed by frequency-domain FWI by Sirgue et al. (2010), whose FWI velocity model can be used as a benchmark to assess our results. The main difference between the FWI formulation of Sirgue et al. (2010) and ours lies in the isotropic time-domain versus VTI frequency-domain formulation of the forward problem. The layout of the 3D wide aperture/azimuth acquisition is shown in Fig. 1a. The targeted area covers a surface of 145 km^2. A recording layout of 12

cables (2302 receivers) recorded 49,954 shots, located 5-m below the sea surface. The nominal distance between cables is 300m, with the two outer cables at 600m. The inline spacing between two consecutive shots and receivers is 50m. We superimpose on the acquisition layout a depth slice of the gas cloud (from this study) to delineate the zone of influence of this gas cloud (Fig. 1a).

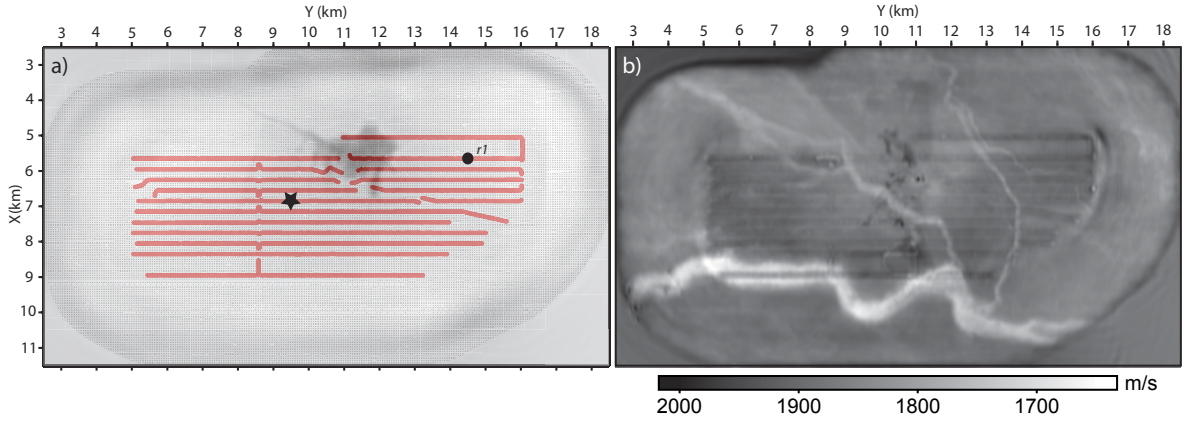

Figure 1 *(a) OBC acquisition layout. A depth slice across the gas cloud is superimposed in transparency. The star and the circle respectively denote the position of the well log (Fig. 2b) and the receiver whose records are shown in Figs. 2a and 4. (b) Depth slice at 175m depth of the final FWI model.*

The seismic wavefield is dominated by the diving waves that propagate above the gas zone (Fig. 2, white arrow), the reflection from the top of the gas layers (Fig. 2, red arrow) and the reflection from the top of the reservoir (Fig. 2, blue arrow).

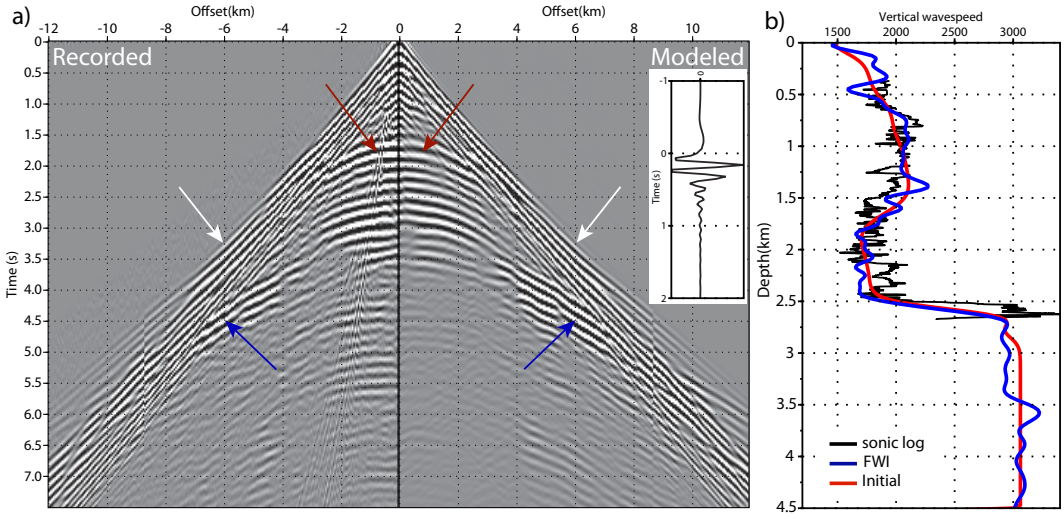

Figure 2 *(a) Receiver gather. The shots are selected along the inline profile running through the receiver position. Left: recorded data. Right: modeled data in the final FWI model. The inset shows the source wavelet that was estimated to match the recorded data and the modeled Green functions. (b) Comparison between well-log (block), reflection tomography (red) and FWI (blue) velocities.*

We sequentially invert 11 frequencies in the 3.5Hz-10Hz frequency band. The grid interval is adapted to the frequency (70m, 50m, 35m for the 3.5Hz-5Hz, 5.2Hz-7Hz, 8Hz-10Hz frequency bands, respectively). All the 49,954 shots and all of the 2302 hydrophones, that are processed in a reciprocal way during seismic modeling, are used at each iteration of the inversion. Seismic modeling is performed with a free surface, meaning that free surface multiples are accounted for during FWI. We only update the vertical wavefield (V_0) during inversion, while the density ρ, the quality factor Q_P and the Thomsen's

parameters δ and ε are kept to their initial values. The initial models for the V_0, δ and ε were built by reflection traveltime tomography (courtesy of BP). The background density model was inferred from the initial V_0 model with the Gardner law while we used a constant $Q_P = 200$ below the sea floor.

An horizontal slice at 175m depth shows a glacial channel system with a remarkable spatial resolution (Fig. 1b). As already noticed by Sirgue et al. (2010) and Warner et al. (2013), the image of the channels extends far beyond the area covered by the cables, suggesting that it was built from refracted waves and/or out-of-plane reflections. Two different perspective views of the V_0 volume highlight the imprint of the gas cloud in the subsurface (Fig. 3). Figure 3a shows a vertical section across the gas cloud, the underlying reservoir and the reflector delineating the base of the cretaceous. A reverse fault cross-cutting the base cretaceous reflector and the reservoir might be interpreted in this Figure. Figure 3b shows a horizontal slice at 1km depth across the gas cloud with a complex network of low-velocity structures radiating out from it. The vertical section across the periphery of the gas cloud shows that these low-velocity structures correspond probably to sub-vertical fractures.

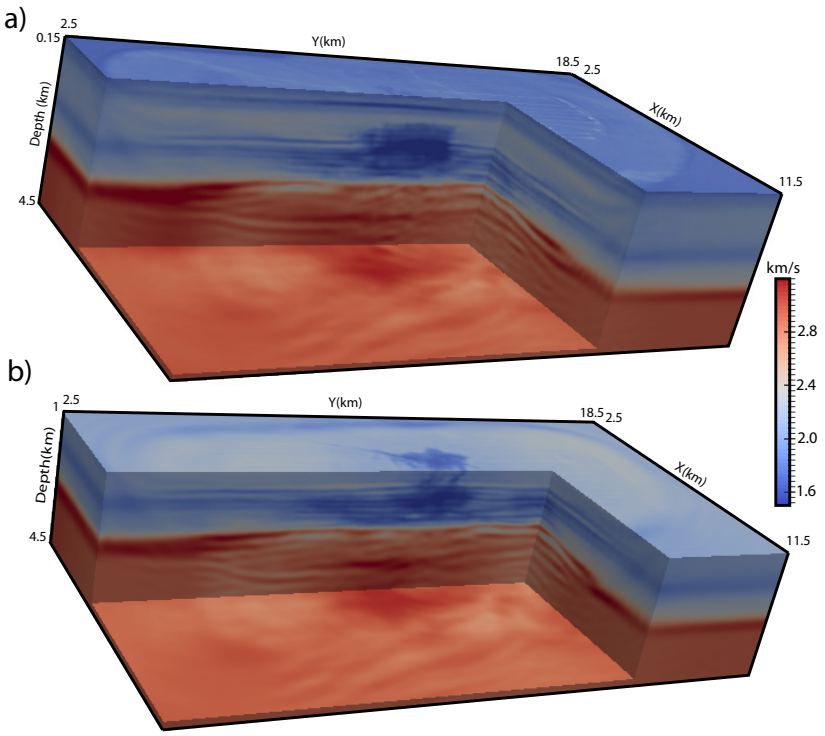

Figure 3 *Final FWI model. (a) View of the gas cloud, the reservoir and the base of the cretaceous. (b) Horizontal slice of the gas cloud and low-velocity structures radiating out from it. The geometry of some low-velocity structures are shown in the vertical plane.*

We assess the relevance of the FWI model by seismic modeling in the time and frequency domains. Comparison between recorded and modeled receiver gathers shows that the FWI model allows us to predict the main arrivals above mentioned (Fig. 2a). The good agreement between the 10Hz recorded and modeled receiver gathers validates the relevance of the VTI visco-acoustic modeling engine for frequency domain FWI (Fig. 4).

The inversion was performed on computer nodes composed of two 2.5GHz Intel Xeon IvyBridge E5-2670v2 processors with 10 cores per processor. The memory per node is 64Gb and the connecting network is infiniband FDR at 56 Gb/s. We submit two MPI processes per node and use 9 threads per MPI process to speedup the basic linear algebra tasks embedded by MUMPS. We used 12, 16 and 34 nodes to process the 70m, 50m and 35m grids, respectively. The number of unknowns in the forward-

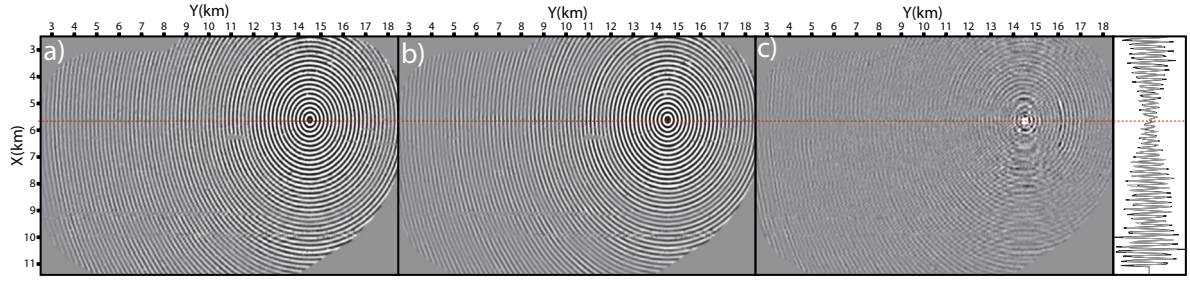

Figure 4 *10-Hz monochromatic recorded (a) and modeled (b) receiver gathers with the difference (c). Direct comparison between recorded (black) and modeled (gray) data are shown in the cross-line direction across the receiver position. A linear gain with offset is applied to balance amplitudes.*

problem linear system is 2.94(70m grid), 7.17(50m grid) and 17.4(35m grid) millions. The memory required by the LU factorization is tractable at these frequencies: 84Gb(70m grid), 288Gb(50m grid), 1.645Tb(35m grid). Although the LU factorization and the multi right-hand sides substitution have the same time complexity ($\mathcal{O}(n^6)$), the cost of the LU factorization is only 11.5%(70m grid), 22%(50m grid), 25%(35m grid) of the cost of the substitution steps. Once the LU factorization is performed, the elapsed time to compute one wavefield solution is only 0.16s(70m grid), 0.37s(50m grid) and 1.1s(35m). The elapsed time to compute one gradient is around 35mn(70m grid), 60mn(50m grid) and 175mn(35m grid). The elapsed times to generate the FWI models after the 7Hz inversion and the 10Hz inversion are around 4.6 days and 6.8 days, respectively.

Conclusions

We show with a real data case study the high computational efficiency of frequency-domain FWI based on sparse direct solver to process fixed-spread ocean-bottom seismic data at low frequencies (3.5Hz-10Hz) with limited computational resources. Pushing frequency-domain FWI at higher frequencies with block-low rank version of MUMPS is part of the future work as well as the extension to multi-parameter reconstruction for ρ, Q_P and ε.

Acknowledgements

This study was partly funded by the sponsors of the SEISCOPE consortium (*http://seiscope2.osug.fr*). This study was granted access to the HPC resources of SIGAMM (http://crimson.oca.eu) and CIMENT computer centers and CINES/IDRIS under the allocation 046091 made by GENCI. We thank BP Norge AS and their Valhall partner Hess Norge AS for allowing access to the Valhall dataset, tomographic models and well-log velocities.

References

Krebs, J. et al. [2009] Fast full-wavefield seismic inversion using encoded sources. *Geophysics*, **74(6)**, WCC105–WCC116.

MUMPS-team [2011] *MUMPS - MUltifrontal Massively Parallel Solver users' guide - version 4.10.0 (May 10, 2011)*. ENSEEIHT-ENS Lyon, http://www.enseeiht.fr/apo/MUMPS/ or http://graal.ens-lyon.fr/MUMPS.

Operto, S., Brossier, R., Combe, L., Métivier, L., Ribodetti, A. and Virieux, J. [2014] Computationally-efficient three-dimensional visco-acoustic finite-difference frequency-domain seismic modeling in vertical transversely isotropic media with sparse direct solver. *Geophysics*, **79(5)**, T257–T275.

Pratt, R.G. [1999] Seismic waveform inversion in the frequency domain, part I : theory and verification in a physic scale model. *Geophysics*, **64**, 888–901.

Sirgue, L., Barkved, O.I., Dellinger, J., Etgen, J., Albertin, U. and Kommedal, J.H. [2010] Full waveform inversion: the next leap forward in imaging at Valhall. *First Break*, **28**, 65–70.

Tarantola, A. [1984] Inversion of seismic reflection data in the acoustic approximation. *Geophysics*, **49**(8), 1259–1266.

Warner, M. et al. [2013] Anisotropic 3D full-waveform inversion. *Geophysics*, **78**(2), R59–R80.